Chinese Chemical Letters 34 (2023) 108129

Contents lists available at ScienceDirect

Chinese Chemical Letters

journal homepage: www.elsevier.com/locate/cclet

A soluble pH-responsive host-guest-based nanosystem for homogeneous exosomes capture with high-efficiency

Haiyan Wang[a,1], Peng Liang[a,1], Lei Zhang[a], Liping Shi[b], Yitong Ge[b], Liyuan Zhang[b,*], Xiaoqiang Qiao[a,*]

[a] College of Pharmaceutical Sciences, Key Laboratory of Public Health Safety of Hebei Province, Key Laboratory of Medicinal Chemistry and Molecular Diagnosis, Ministry of Education, Hebei University, Baoding 071002, China
[b] College of Basic Medical Science, Key Laboratory for Proteomics of Liaoning Province, Dalian Medical University, Dalian 116044, China

ARTICLE INFO

Article history:
Received 31 August 2022
Revised 24 November 2022
Accepted 1 January 2023
Available online 5 January 2023

Keywords:
Exosomes
Homogeneous capture
Soluble nanosystem
pH-responsive polymer
Host-guest interaction

ABSTRACT

Exosomes offer ideal biomarkers for liquid biopsies. However, high-efficient capture of exosomes has been proven to be extreme challenging. Here, we report a soluble pH-responsive host-guest-based nanosystem (pH-HGN) for homogeneous isolation of exosomes around physiological pH. The pH-HGN consists of two specifically functionalized modules. First, a pH-responsive module, poly-dimethylaminoethyl methacrylate, provides homogeneous capture circumstances and sharp pH-triggered self-assembly separation in aqueous solution to improve capture efficiency and reduce nonspecific adsorption. Second, a host-guest module, poly-acrylamide azobenzene and β-cyclodextrin linked with exosomes-specific antibody, could act as the "cleavable bridge" to specific capture and subsequent rapid release of captured exosomes through host-guest interaction between β-cyclodextrin and AAAB moieties. The pH-HGN offered high capture efficiencies for exosomes from two different cell lines, which were 90.2% ± 0.28% and 87.0% ± 4.6% for H1299 and MCF-7 cell-derived exosomes, respectively. The purity of isolated exosomes was $(1.49 \pm 0.71) \times 10^{11}$ particles/μg, which was 4.1 times higher compared with the gold standard ultracentrifugation (UC) method. Furthermore, the isolated exosomes *via* the pH-HGN can preserve well integrity and biological activity. The developed pH-HGN was further successfully applied to differentiate lung cancer patients from healthy persons. These findings indicated that pH-HGN is a promising strategy in exosomes-based research and downstream applications.

Exosomes are small (30–150 nm), cell-secreted phospholipid bilayers vesicles [1,2], which modulate a variety of cellular functions, including signal transduction [3,4], drug resistance [5], immune response [6], cancer progression and metastasis [7,8]. Recently, exosomes-based liquid biopsies have emerged as a non-invasive, sensitive, real-time specific and cost-effective cancer diagnosis [9,10], as they contain tumor-specific proteins and nucleic acids. However, the lack of efficient and robust technologies to isolate intact exosomes from biological fluids seriously restricts their biomedical and clinical implementation.

To date, isolation approaches, such as ultracentrifugation (UC), gradient ultracentrifugation, co-precipitation, size-exclusion chromatography as well as microfluidic-based techniques have been developed for exosomes isolation [11–16]. For example, UC is served as the "gold standard" for exosomes purification. However, this method is time consuming and often of low isolation efficiency [17]. The polymer co-precipitation strategy based on commercial kits can be used for reproducible isolation of exosomes with low centrifugal forces. However, the method can also co-precipitate miRNA and lipoproteins [18]. Currently, immunoaffinity capture strategies have also been widely utilized for exosomes isolation due to the advantages of high specificity, capacity, and facileness to be incorporated into downstream analysis. As such, exosomes-specific antibodies or exosomes-binding molecules were exploited to be immobilized on solid supports, like beads [19,20], metal-organic frameworks [21] or microfluidic chips [22–24] to isolate exosomes in heterogeneous conditions. However, due to their heterogeneous natures, the solid matrix-based approaches suffer from interfacial mass transfer resistance, high steric hindrance and nonlinear binding dynamics [25–28]. When dealing with extremely low abundance exosomes, it can yield low recovery, poor reproducibility, and high non-specific adsorption.

* Corresponding authors.
E-mail addresses: zhiani@126.com (L. Zhang), xiaoqiao@hbu.edu.cn (X. Qiao).
[1] These authors contributed equally to this work.

https://doi.org/10.1016/j.cclet.2023.108129
1001-8417/

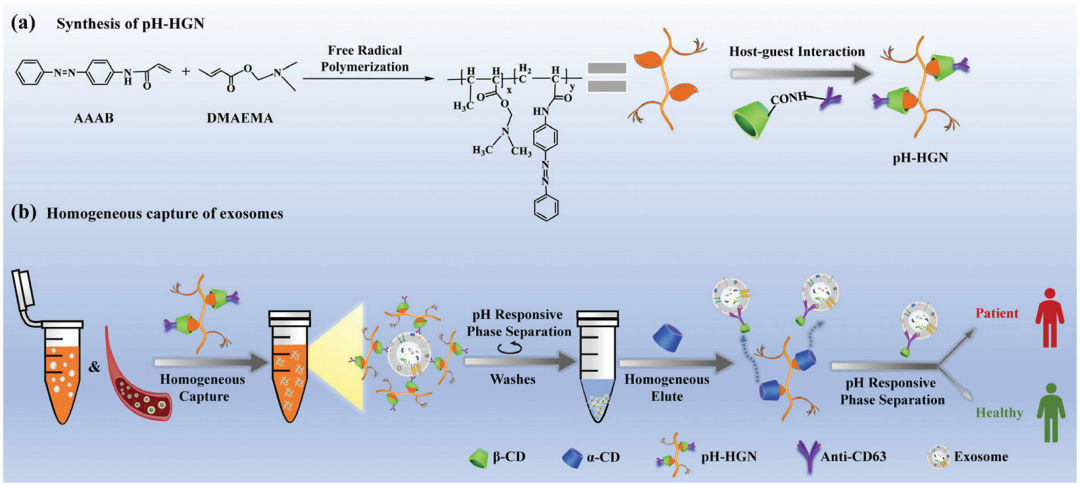

Scheme 1. The schematic overview of synthesis and application of the pH-HGN for exosomes isolation.

To address this, we designed a soluble pH-responsive host-guest-based nanosystem (pH-HGN) which offers homogeneous capture and rapid recovery of intact exosomes with high-efficiency. The soluble pH-HGN was prepared by copolymerization of pH-responsive monomer with host-guest modules. First, dimethylaminoethyl methacrylate (DMAEMA) was chosen as the pH-responsive monomer, due to its capacity to enable the designed pH-HGN a sharp pH-triggered self-assembly in aqueous solution with rapid phase separation around physiological pH [29–31]. This is vital for maintaining the biological function of exosomes. For the host-guest modules, another monomer, acrylamide azobenzene (AAAB) (Figs. S1 and S2 in Supporting information), was used as the "cleavable bridge" [20,32]. As shown in Scheme 1, the poly(DMAEMA-*co*-AAAB) was successfully synthesized with DMAEMA and AAAB as the monomers *via* free radical polymerization. The pH-HGN was formed by further introducing carboxymethyl-β-cyclodextrin sodium salt (β-CD)-anti-CD63 antibody *via* host-guest noncovalent interactions between β-CD and AAAB. The pH-HGN could provide homogeneous circumstances for exosomes capture in aqueous solution around physiological pH. Then, simply by raising the system pH, facile and efficient exosomes isolation can be achieved by rapid self-assembly of pH-HGN-exosomes conjugates. Last, α-cyclodextrin (α-CD), a biofriendly competition agent, was chosen to readily release exosomes from pH-HGN through host-guest interaction in homogeneous condition. The isolated exosomes can be further exploited for clinical downstream analysis. In comparison with the conventional solid/insoluble matrix based exosomes isolation approaches, our developed pH-HGN possesses three potential merits. First, the soluble nature of the pH-HGN can substantially reduce the steric hindrance effect which benefits for trace exosomes capture. Second, the pH-responsive chains in pH-HGN exhibit rapid and reversible pH-induced phase transition around physiological pH. The agglomerates of the pH-HGN could be obviously visualized and then precipitated from solution with low-speed centrifugation. Last, host-guest noncovalent interactions have been introduced as smart "cleavable bridges" for exosomes release, which provides facile and convenient exosomes recovery without damage [20].

The compositions of the poly(DMAEMA-*co*-AAAB) were designed to have phase transitions triggered near physiological pH. As shown in Table S1 (Supporting information), the copolymer with higher monomer ratio of DMAEMA was found to have a higher pK_a, which may be attributed to the elevated ratio of amine. The copolymer with pK_a of 6.5 was chosen for further investigation. The successful synthesis of poly(DMAEMA-*co*-AAAB) was validated by Fourier transform infrared (FT-IR). The characteristic peaks at 2950 cm^{-1} and 2830 cm^{-1} correspond to the symmetric and asymmetric C-H stretching vibrations of methyl in DMAEMA monomer, while the peaks at 1600 cm^{-1} and 1500 cm^{-1} are assigned to phenyl groups in AAAB monomer (Fig. S3a in Supporting information). Fig. S3b (Supporting information) shows the ^{1}H NMR spectrum of the copolymer. The signals of aromatic protons at 8.0–7.4 ppm and methyl protons at 2.4–2.2 ppm confirm the presence of azobenzene and tertiary amine units in the copolymer. The molar ratio of AAAB to DMAEMA in the copolymer was calculated to be 1:1.2 from the integration of the aromatic and methyl proton signals. Matrix-assisted laser desorption ionization-time of flight mass spectrometry (MALDI-TOF MS) was further used to determine the molecular weight of the copolymer. As shown in Fig. 1a, the copolymer displayed a molecular weight about 347 kDa with low polydispersity. The transmission electron microscope (TEM) image shows that the poly(DMAEMA-*co*-AAAB) is of amorphous shape with a diameter about 50–100 nm (Fig. 1b).

Narrow pH responsive range and high responsive sensitivity can help to improve the sample recovery in subsequent exosomes isolation procedures. Therefore, the pH-responsive properties of poly(DMAEMA-*co*-AAAB) were evaluated by optical transmittance experiments. As shown in Fig. 1c, after changing the pH from 7.0 to 7.5, the transparent yellow copolymer solution immediately turned into turbid yellow suspension due to aggregation. The yellow color originated from AAAB. The copolymer precipitates can be easily separated by centrifugation at 3000 *g* for 10 min (Fig. 1d). Furthermore, the transparency of the copolymer solution was investigated by UV adsorption analysis in the pH range of 5.5–8.0. As shown in Fig. 1e, at pH 6.5, the copolymer completely dissolved with solubility calculated as 97.2% $\pm$ 2.4%. The aggregation was triggered at the critical pH value (pK_a at 6.5) and the turbidity of the polymer solution increased sharply. After changing the pH to 7.5, over 98.0% $\pm$ 0.7% copolymer had been precipitated. These results proved that the copolymer displayed a sharp pH-triggered phase transition, where the turbidity from 0 to 100% was limited to 1 pH unit. Since repeated washing steps are required to remove the non-specifically adsorbed biomolecules, the reversibility of the copolymer was also investigated. As shown in Fig. 1f, the copolymer can switch between dissolution and aggregation reversibly and repeatedly by variation pH between 6.0 and 8.0 for at least six cycles. All these results indicated that the poly(DMAEMA-*co*-AAAB) could potentially facilitate exosomes capture with rapid responsiveness under physiological conditions.

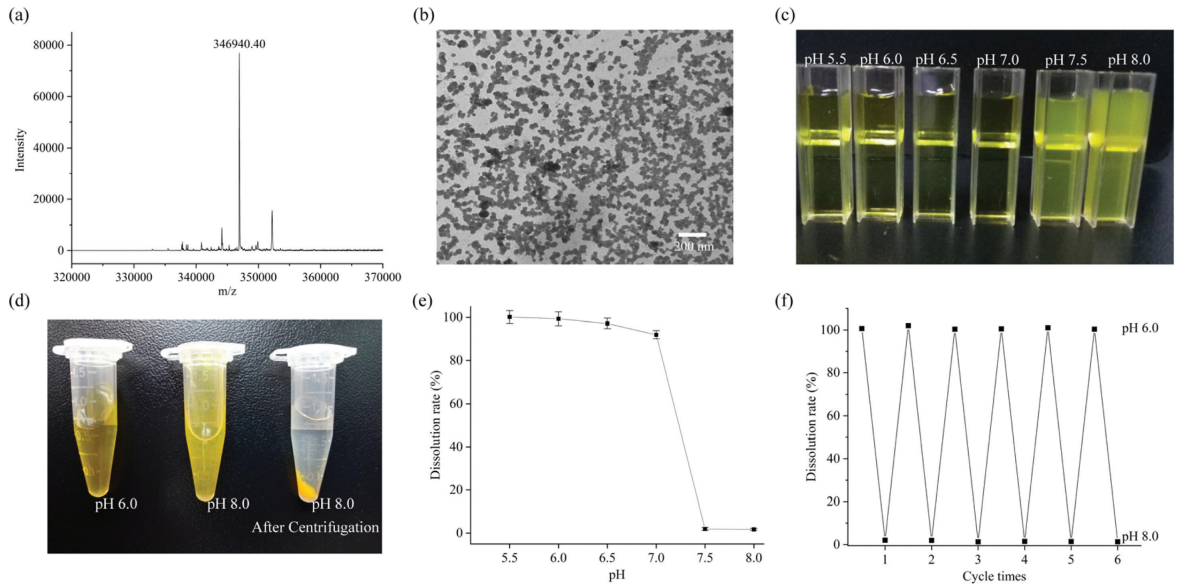

Fig. 1. Characterization of the poly(DMAEMA-*co*-AAAB): MALDI-TOF mass spectrum (a) and TEM image (b) of poly(DMAEMA-*co*-AAAB). (c) Optical images of poly(DMAEMA-*co*-AAAB) solutions at different pH (5.5–8.0). (d) Visualization of pH-triggered phase transition of poly(DMAEMA-*co*-AAAB) at pH 8.0 and the copolymer precipitation after centrifugation. (e) The turbidity-pH response curve of the poly(DMAEMA-*co*-AAAB). (f) The pH reversibility of poly(DMAEMA-*co*-AAAB) between pH 6.0 and pH 8.0.

The phase separation efficiency of poly(DMAEMA-*co*-AAAB) (10 mg/mL) at pH 7.5 was investigated under different centrifugal forces and centrifugation time. As shown in Fig. S4a (Supporting information), higher *g*-force and longer centrifugation time contribute to lower residual rates of poly(DMAEMA-*co*-AAAB) in solution, which was about 1.6% ± 0.20% after centrifugation at 3000 *g* for 10 min, indicating a high phase separation efficiency of over 98.0%. Further increasing the centrifugal force or extending the centrifugation time has no significant effect on the phase separation efficiency. Besides, the concentration of poly(DMAEMA-*co*-AAAB) also has no significant effect on the phase separation efficiency after centrifugation at 3000 *g* for 10 min (Fig. S4b in Supporting information). These results show that high phase separation efficiency can be achieved in 10 min when the centrifugation is performed over 3000 *g*.

Protein antifouling is an important factor for matrix material in the capture of exosomes. The antifouling property of poly(DMAEMA-*co*-AAAB) was firstly evaluated with human serum albumin (HSA) and bovine serum albumin (BSA) as the model samples. The concentrations of HSA and BSA were chosen as high as 10 mg/mL. As shown in Fig. S5 (Supporting information), after 1 h incubation of poly(DMAEMA-*co*-AAAB) with HSA or BSA solution, and three washes with 1 mL PBS buffer, only 0.012% ± 0.006% of the original HSA and 0.02% ± 0.002% of BSA were found, respectively. Exosome-free human serum was further used to evaluate the anti-contamination effect in real biological samples. The residual protein in the third wash was only 0.094% ± 0.001% of the initial solution. These results indicate that, despite the high content of protein in the incubation solution, the copolymer still showed excellent antifouling ability, which facilitates to improve isolated purity of exosomes.

Immunofluorescence experiments were performed to confirm the successful immobilization of anti-CD63 antibody using FITC-labeled goat anti-rabbit IgG. As shown in Fig. S6a (Supporting information), no fluorescence signal was observed for direct detection of poly(DMAEMA-*co*-AAAB). Similarly, without conjugation of anti-CD63 antibody, no fluorescence signal was detected on the poly(DMAEMA-*co*-AAAB) after incubation with the fluorescent second antibody (Fig. S6b in Supporting information). This result can also demonstrate the super antifouling ability of the copolymer. After introducing of anti-CD63 antibody on poly(DMAEMA-*co*-AAAB), the pH-HGN was obtained, which exhibited bright green fluorescence after incubation with the fluorescent second antibody (Fig. S6c in Supporting information). These results confirm the successful anti-CD63 antibody decoration. Additionally, quantitative investigation of anti-CD63 antibody immobilized on the pH-HGN was executed by the BCA protein quantification kit through the depletion method [33]. The amount of conjugated anti-CD63 antibody on poly(DMAEMA-*co*-AAAB) (10 mg) was calculated to be about 5.17 ± 0.59 μg. The immobilization efficiency of anti-CD63 antibody was about 85.0% ± 1.5%.

To optimize the extraction efficiency of the pH-HGN based strategy, the amount of pH-HGN and the incubation time were investigated. The supernatants (4 mL) harvested from H1299 cell (seeded 5×10^5 cell/per 36 cm^2 flask) at 48 h were used as the model sample. The exosomes isolation efficiency [34] was optimized according to the amount of total exosomal proteins extracted from the exosomes isolated by pH-HGN. As the amount of pH-HGN increasing from 2.0 mg to 16.0 mg, exosomal proteins eluted from pH-HGN sharply increased to the maximum at 10 mg pH-HGN (Fig. S7a in Supporting information). Further increasing the amount of pH-HGN, the capture efficiency slightly decreased. For the incubation time, the capture efficiency gradually increased and reached to the maximum in 40 min (Fig. S7b in Supporting information). Extended incubation time did not further increase the capture efficiency. Thus, the optimal amounts of pH-HGN and incubation time were 10 mg and 40 min, respectively.

Under the optimal conditions, the exosomes isolated by pH-HGN from H1299 culture medium was characterized by TEM. As shown in Fig. 2a, the exosomes captured on the surface of pH-HGN could be obviously observed. In addition, intact and well-dispersed exosomes could be robustly recovered by simple elution process and a typical phospholipid bilayer structure was revealed (Fig. 2b). The purified exosomes displayed a single peak at approximate 123.23 ± 0.51 nm as determined by nanoparticle tracking analysis (NTA) (Fig. 2c). The enrichment of typical exosomal markers HSC70, TSG101, CD81 and CD9 was confirmed by western blot. As shown in Fig. 2d, the expression levels of these proteins were undetectable in the cell culture medium before enrichment and supernatant. However, after isolation with pH-HGN, all of the four

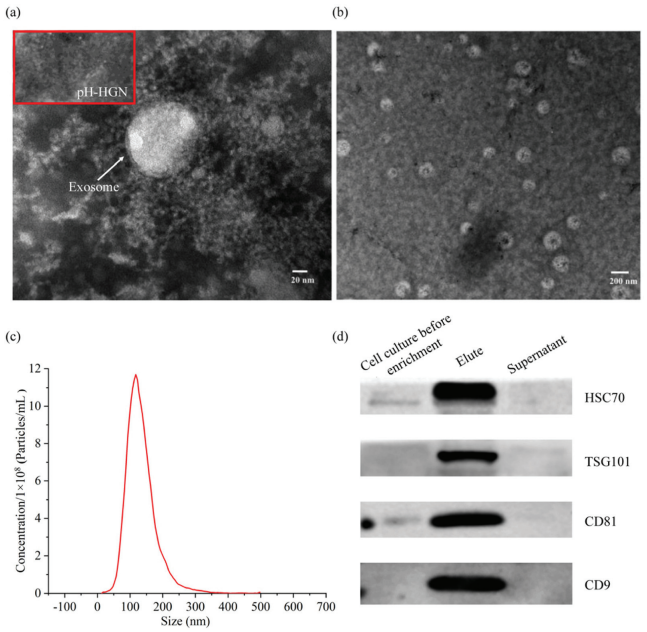

Fig. 2. Representative TEM images of pH-HGN (inset image in a) and intact H1299 cells-derived exosomes captured on (a) and eluted (b) from pH-HGN. (c) The size distribution of H1299 cells-derived exosomes profiled by NTA analysis. (d) Western blot analysis of H1299 cells-derived exosomal markers HSC70, TSG101, CD81 and CD9.

proteins were clearly identified in the elution. In addition, the isolation efficiencies of pH-HGN for H1299 and MCF-7 cell-derived exosomes were 90.2% ± 0.28% and 87.0% ± 4.60%, respectively, proving the good reliability and broader possibilities of pH-HGN for different types of tumor cells. The capture efficiencies of pH-HGN are comparable or higher than that of the recently reported methods (Table S2 in Supporting information). The improved capture efficiencies for trace exosomes achieved by the developed pH-HGN is mainly due to the homogeneous enrichment nature, which could offer good site accessibility and low mass transfer resistance. Besides, the elution protocol based on host-guest interactions also provides a biofriendly and efficient strategy.

UC is considered as the gold standard technique to isolate exosomes from biological fluid. The developed pH-HGN was further compared with the UC technique. First, the size and the total number of exosomes obtained from H1299 cell supernatant were comparatively analyzed according to the NTA measurements. As shown in Fig. 3a, high amount of exosomes were successfully captured by pH-HGN, which derived from the high captured efficiency of the developed pH-HGN. Moreover, a significantly higher ratio of exosomes was present in the expected size range (30–150 nm) compared that *via* the UC technique (Fig. 3b). Second, elevated levels of exosomal marker proteins were also successfully recognized *via* the developed pH-HGN. As shown in Fig. 3c, compared with the UC technique, high abundance exosomal markers HSC70, TSG101, CD81, and CD9 could be easily identified after enrichment by pH-HGN. The relative amounts of the exosomal markers HSC70, TSG101, CD81, and CD9 recovered by the pH-HGN were approximate 3.6, 2.9, 8.8, and 2.0-fold of that *via* the UC technique (Fig. 3d). The purity of captured exosomes has been proposed to be defined as the ratio of particle counts to contaminating protein amount [35,36], which can be calculated based on the NTA and BCA data. Our results revealed that the pH-HGN yielded more exosomes than *via* UC (Fig. 3e). As far as the purity was concerned, pH-HGN offered the purity as $(1.49 \pm 0.71) \times 10^{11}$ particles/μg, whereas UC offered $(3.62 \pm 0.31) \times 10^{10}$ particles/μg. The purity of exosomes obtained by pH-HGN was 4.1 times higher than that *via* UC technique (Fig. 3f). Therefore, with the developed pH-HGN, high purity of exosomes could be obtained with higher yield.

To examine the biological activity of exosomes isolated by pH-HGN *in vitro*, a colony formation assay was performed to evaluate the proliferative ability of H1299 cells after treatment with exosomes. The results showed that the exosomes treated cells formed significantly more colonies in a dose-dependent manner compared with the control group at 7 days (Fig. S8 in Supporting information). Furthermore, the cell proliferation experiment was also performed. The H1299 cells were treated with absence or in the presence of different concentrations (10^6, 10^8, 10^{10}, 10^{12} particles/well) of exosomes derived from H1299 cells for 24, 48 or 72 h. The proliferation of cells was examined by CCK-8 analysis. As shown in Fig. S9 (Supporting information), the exosomes isolated by pH-HGN could significantly promote proliferation of H1299 cells in both time-dependent and dose-dependent manners. Meanwhile, the effect of exosomes on apoptosis was also investigated by flow cytometric annexin-V binding assay. H1299 cells were treated with absence or in the presence of different concentrations (10^8, 10^{10} particles/well) of exosomes for 48 h, respectively. As shown in Fig. S10 (Supporting information), the cell apoptosis rates were decreased in exosomes treated groups compared with the control group ($P < 0.01$), which demonstrated the inhibitory effect of exosomes on cell apoptosis. All these results demonstrated that the exosomes isolated by pH-HGN possess various biological activities.

Lung cancer remains the leading cause of cancer-related death in China [37–39]. Early screening holds great promise to improve the survival rates of lung cancer patients. Recently, serum derived exosomes have become an emerging interest for early diagnosis of cancer, since exosomes carry a wide variety of biomarkers and the level of circulating exosomes is elevated in cancer patients [9-12,40]. The applicability of pH-HGN for complex human serum samples was studied. As shown in Fig. S11 (Supporting information), the successful isolation of exosomes with high efficiency was also achieved *via* pH-HGN approach. In addition, the purity of isolated exosomes was evaluated with albumin (ALB), as ALB is the most abundant circulating protein in plasma and the main contaminant in exosomes isolation [41,42]. The result revealed that non-exosome components hardly co-isolated with exosomes. The clinical feasibility of the developed pH-HGN was further investigated by isolation and analysis of exosomes in the human serum of 7 lung cancer patients with different pathologic types and stages (7 healthy donors as the controls). The concentrations of exosomes in the lung cancer group and healthy control group were first evaluated with NTA, which were $(6.27 \pm 0.31) \times 10^9$ and $(1.51 \pm 0.06) \times 10^9$ particles/mL, respectively. The NTA data revealed that the concentration of exosomes in lung cancer patients was more than 4 folds higher than those from the healthy persons. The up-regulated expressions of HSC70, TSG101 and CD81 in exosomes are often associated with many cancer types, including lung cancers. As shown in Fig. 4, the expression of exosomal markers including HSC70, TSG101 and CD81 were detected by Western blot. The expression levels of these marker proteins in serum exosomes from lung cancer patients significantly exceeded those in serum exosomes from healthy persons. These results further confirmed the findings that the developed pH-HGN can exclusively capture target exosomes, which show good application potential in medical and biological science.

In summary, a novel pH-responsive host-guest-based nanosystem, pH-HGN, was successfully developed for homogeneous capture and efficient recovery of trace exosomes. The soluble pH-responsive nature of pH-HGN enabled a homogeneous immune-affinitive capture and mild elution of intact exosomes around physiological pH with high efficiency and purity. Consequently, this unique pH-HGN could provide a new tool for liquid biopsy-based companion diagnostic assays.

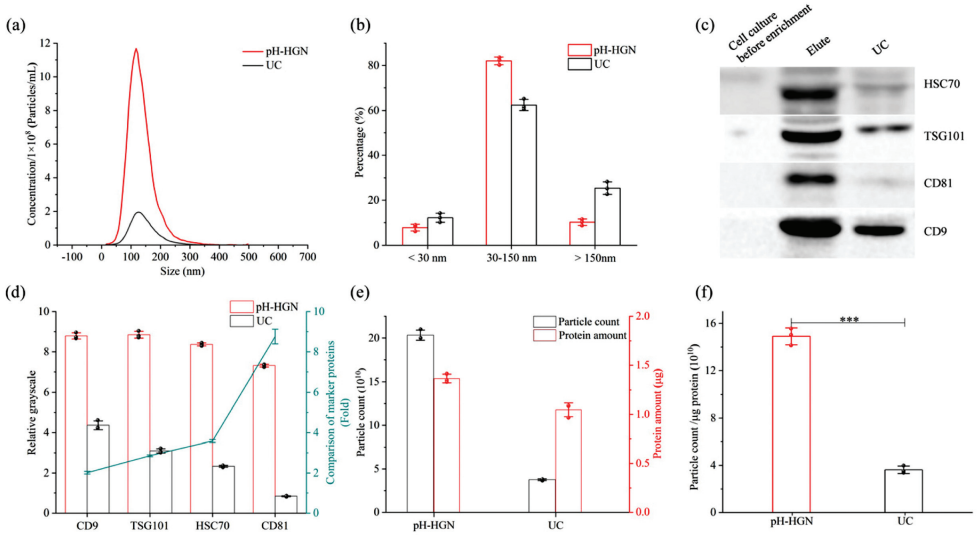

Fig. 3. Comparison of the exosomes isolated *via* the pH-HGN and UC technique: Size distribution (a), size distribution percentage (b), Western blot analysis (c) and relative abundance (d) of exosomal markers HSC70, TSG101, CD81, and CD9. (e) Particle count and contaminating protein amount. (f) Ratio of particle count to contaminating protein amount. All the experiments were performed at least 3 times and representative images are shown. The data are expressed as the mean ± SD, $^{***}P < 0.001$.

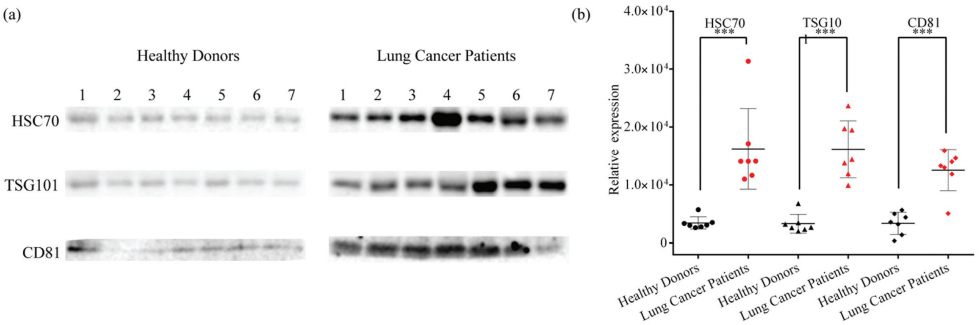

Fig. 4. Western blot (a) and relative quantification (b) of exosomal marker proteins in clinical samples. Data are reported as mean ± SD, $n = 7$ in each group. $^{***}P < 0.001$.

Declaration of competing interest

The authors declare that they have no known competing financial interests or personal relationships that could have appeared to influence the work reported in this paper.

Acknowledgments

This work is financially supported by National Natural Science Foundation of China (Nos. 21974017, 22274035), Liaoning Revitalization Talents Program (No. XLYC2007122), Natural Science Foundation of Hebei Province (No. B2019201327), Hundred Outstanding Innovative Talents in Universities of Hebei Province (No. SLRC2019016), Young Talent of Hebei Province, Natural Science Interdisciplinary Research Program of Hebei University (No. DXK201912, DXK202014), Liaoning Provincial Natural Science Foundation of China (No. 2020-MS-261) and Program in Liaoning Province Education Department (No. LZ2019063).

Supplementary materials

Supplementary material associated with this article can be found, in the online version, at doi:10.1016/j.cclet.2023.108129.

References

[1] M.P. Bebelman, P. Bun, S. Huveneers, et al., Nat. Protoc. 15 (2020) 102–121.
[2] H. Xu, C. Liao, P. Zuo, Z. Liu, B. Ye, Anal. Chem. 90 (2018) 13451–13458.
[3] L. Zheng, H. Wang, P. Zuo, et al., Anal. Chem. 94 (2022) 7703–7712.
[4] K. Mori, M. Hirase, T. Morishige, et al., Angew. Chem. Int. Ed. 58 (2019) 1612–1615.
[5] J. Wang, A. Hendrix, S. Hernot, et al., Blood 124 (2014) 555–566.
[6] M. Poggio, T. Hu, C.C. Pai, et al., Cell 177 (2019) 414–427.
[7] W. Sun, Y. Ren, Z. Lu, X. Zhao, Mol. Cancer 19 (2020) 135.
[8] W. Feng, D.C. Dean, F.J. Hornicek, H. Shi, Z. Duan, Mol. Cancer 18 (2019) 124.
[9] Y. Lu, Z. Tong, Z. Wu, et al., Chin. Chem. Lett. 33 (2022) 3188–3192.
[10] K. Jiang, Y. Wu, J. Chen, et al., Chin. Chem. Lett. 32 (2021) 1827–1830.
[11] Z. Han, X. Peng, Y. Yang, et al., Biosens. Bioelectron. 217 (2022) 114709.
[12] Z. Han, C. Peng, J. Yi, et al., Sens. Actuators B: Chem. 333 (2021) 129563.
[13] H. Xie, K. Di, R. Huang, et al., Chin. Chem. Lett. 31 (2020) 1737–1745.
[14] H. Shao, H. Im, C.M. Castro, et al., Chem. Rev. 118 (2018) 1917–1950.
[15] H. Zheng, S. Guan, X. Wang, et al., Anal. Chem. 92 (2020) 9239–9246.
[16] R.J. Lobb, M. Becker, S.W. Wen, et al., J. Extracell. Vesicles 4 (2015) 27031.
[17] F. Momen-Heravi, Methods Mol. Biol. 1660 (2017) 25–32.
[18] K. Rekker, M. Saare, A.M. Roost, et al., Clin. Biochem. 47 (2014) 135–138.
[19] H. Qi, C. Liu, L. Long, et al., ACS Nano 10 (2016) 3323–3333.
[20] S. Cai, B. Luo, P. Jiang, et al., Nanoscale 10 (2018) 14280–14289.
[21] L. Zhang, H. Wang, G. Zhao, et al., Anal. Chem. 93 (2021) 6534–6543.
[22] S.S. Kanwar, C.J. Dunlay, D.M. Simeone, S. Nagrath, Lab Chip 14 (2014) 1891–1900.
[23] P. Li, M. Kaslan, S.H. Lee, J. Yao, Z. Gao, Theranostics 7 (2017) 789–804.
[24] F.S. Iliescu, D. Vrtačnik, P. Neuzil, C. Iliescu, Micromachines (Basel) 10 (2019) 392.
[25] L. Wang, L. Yang, L. Pan, et al., J. Am. Chem. Soc. 137 (2015) 12772–12775.
[26] H. Bai, C. Fan, W. Zhang, et al., Chem. Sci. 6 (2015) 4234–4241.
[27] L. Zhang, H. Jiang, J. Yao, et al., Chem. Commun. 50 (2014) 1027–1029.
[28] Y. Chen, J. Tong, J. Dong, J. Luo, X. Liu, Small 15 (2019) 1900099.
[29] A.E. Smith, X. Xu, S.E. Kirkland-York, D.A. Savin, C.L. McCormick, Macromolecules 43 (2010) 1210–1217.
[30] M.T. Savoji, S. Strandman, X.X. Zhu, Langmuir 29 (2013) 6823–6832.
[31] L. Xu, H.L. Li, L.P. Wang, Polymers (Basel) 11 (2019) 2026.
[32] J.L. Zhu, K.L. Liu, Y. Wen, X. Song, J. Li, Nanoscale 8 (2016) 1332–1337.
[33] Z. Feng, Q. Guo, Y. Wang, et al., ACS Omega 7 (2022) 2344–2355.

[34] N. Ludwig, B.M. Razzo, S.S. Yerneni, T.L. Whiteside, Exp. Cell Res. 378 (2019) 149–157.
[35] J. Webber, A. Clayton, J. Extracell. Vesicles 2 (2013) 19861.
[36] H.K. Woo, V. Sunkara, J. Park, et al., ACS Nano 11 (2017) 1360–1370.
[37] R.L. Siegel, K.D. Miller, H.E. Fuchs, A. Jemal, CA Cancer J. Clin. 71 (2021) 7–33.
[38] W. Chen, R. Zheng, P.D. Baade, et al., CA Cancer J. Clin. 66 (2016) 115–132.
[39] R.M. Feng, Y.N. Zong, S.M. Cao, R.H. Xu, Cancer Commun. 39 (2019) 22.
[40] L. Cheng, A.F. Hill, Nat. Rev. Drug Discov. 21 (2022) 379–399.
[41] C. Thery, K.W. Witwer, E. Aikawa, et al., J. Extracell. Vesicles 7 (2018) 1535750.
[42] N. Karimi, A. Cvjetkovic, S.C. Jang, et al., Cell. Mol. Life Sci. 75 (2018) 2873–2886.